Accepted Manuscript

3D printed spacers for organic fouling mitigation in membrane distillation

Erik Hugo Cabrera Castillo, Navya Thomas, Oraib Al-Ketan, Reza Rowshan, Rashid K. Abu Al-Rub, Seongchul Ryu, Duc Long Nghiem, Saravanamuthu Vigneswaran, Hassan A. Arafat, Gayathri Naidu

PII: S0376-7388(19)30201-7

DOI: https://doi.org/10.1016/j.memsci.2019.03.040

Reference: MEMSCI 16941

To appear in: *Journal of Membrane Science*

Received Date: 24 January 2019

Revised Date: 12 March 2019

Accepted Date: 13 March 2019

Please cite this article as: E.H.C. Castillo, N. Thomas, O. Al-Ketan, R. Rowshan, R.K. Abu Al-Rub, S. Ryu, D.L. Nghiem, S. Vigneswaran, H.A. Arafat, G. Naidu, 3D printed spacers for organic fouling mitigation in membrane distillation, *Journal of Membrane Science* (2019), doi: https://doi.org/10.1016/j.memsci.2019.03.040.

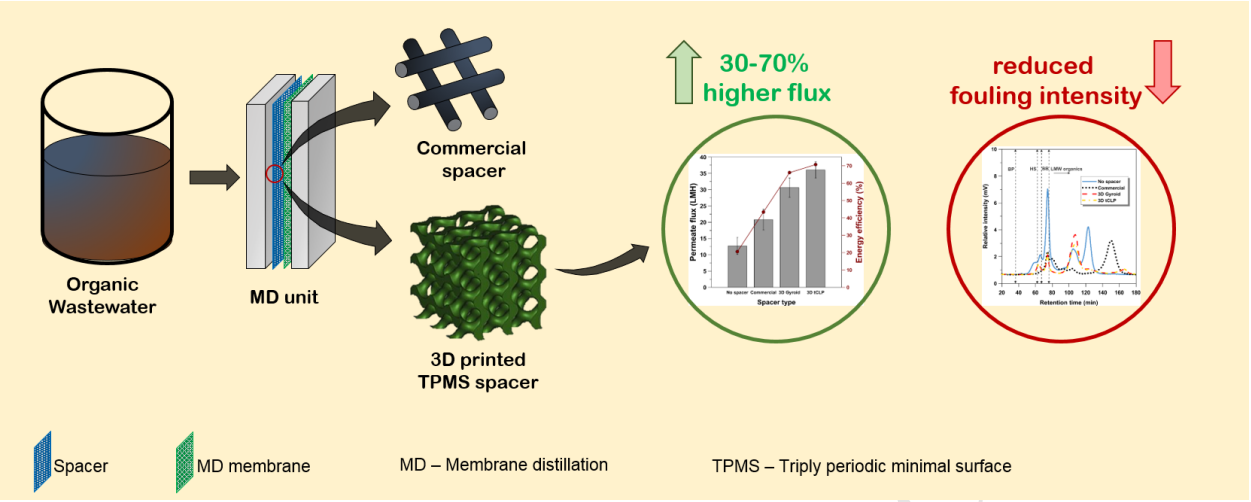

3D printed spacers for organic fouling mitigation in membrane distillation

Erik Hugo Cabrera Castillo[a,b,1], Navya Thomas[c,1], Oraib Al-Ketan[c], Reza Rowshan[d], Rashid K. Abu Al-Rub[c], Seongchul Ryu[a], Duc Long Nghiem[a], Saravanamuthu Vigneswaran[a], Hassan A. Arafat[c,*], Gayathri Naidu[a,*]

[a] School of Civil and Environmental Engineering, University of Technology Sydney (UTS), City Campus, Broadway, NSW 2007, Australia,

[b]Water Management and Technology Center, University of La Frontera (UFRO), Temuco, Chile

[c]Center for Membrane and Advanced Water Technology, Khalifa University of Science and Technology, Abu Dhabi, United Arab Emirates

[d] Core Technology Platforms, New York University Abu Dhabi, Abu Dhabi, UAE

[1]E. Castillo and N. Thomas contributed equally to this work

*Corresponding authors: Email: Gayathri.Danasamy@uts.edu.au (G.Naidu); Hassan.arafat@ku.ac.ae (H. Arafat)

Abstract

3D printing offers the flexibility to achieve favourable spacer geometrical modification. The role of 3D printed spacers for organic fouling mitigation in direct contact membrane distillation (DCMD) is evaluated. Compared to a commercial spacer, the design of 3D printed triply periodic minimal surfaces spacers (Gyroid and tCLP) - varying filament thickness and smaller hydraulic diameter enhanced DCMD fluxes by 50-65%. The highest DCMD flux was obtained with the 3D tCLP spacer due to its specific geometrical design feature. However, its design characteristics resulted in higher channel pressure drop compared to 3D Gyroid spacer. Moreover, 3D Gyroid spacer exhibited superior fouling mitigation (lower membrane organic mass deposition and reversible membrane hydrophobicity with humic acid solution), attributed to its tortuous design that repelled foulants. 3D Gyroid spacer was effective in achieving high water recovery (85%) while maintaining good quality distillate (10-15 μS/cm, 99% ion rejection) in DCMD with wastewater concentrate that contained high organics, mixed with inorganics. In MD, high organic contents minimally affected MD fluxes but reduced membrane hydrophobicity. Repeated DCMD cycles showed that organic pre-treatment as well as cleaning-in-place of membrane and spacer are essential for achieving high recovery rate while maintaining a stable long-term DCMD operation with wastewater concentrate.

Keywords: Organic fouling; membrane distillation; 3D printed spacers; triply periodic minimal surfaces; wastewater.

1. Introduction

Membrane distillation (MD) is a thermal integrated membrane process driven by a vapour pressure gradient across a microporous and hydrophobic membrane [1, 2]. As a phase separation process, MD produces high quality permeate (distillate) with a good recovery due to its insensitivity to osmotic pressure of a highly saline solution [3]. The energy requirement for MD can be met by waste heat from the industry [3]. These factors have led to a focus on the application of MD as an alternative treatment process for wastewater [4], seawater [5] and other saline solutions from the industry [6].

Direct contact MD (DCMD) is the most frequently studied MD configuration due to its simplicity [3, 7]. In the DCMD configuration, the hot feed and cold distillate streams are in direct contact with the membrane, thus, heat conduction and temperature polarization are significant factors governing the energy efficiency. Several operational approaches have been explored to reduce the impact of temperature polarization and increase the overall performance of DCMD, such as improving the hydrodynamic conditions at the membrane surface by increasing the circulation flow rate or generating a suction (vacuum) on the distillation side [8, 9]. Another noteworthy approach is to improve the design of the membrane spacer. Previous studies have shown that spacers act as static turbulence promoter to enhance the efficiency of transmembrane mass transfer, thereby, increasing permeate fluxes by up to 60% compared to an empty channel [10-14].

1.1 3D printed spacers for MD

The effectiveness of spacers is highly dependent on factors such as mesh design, thickness, flow attack angle, and materials. The onset of 3D printing has enabled the fabrication of novel spacers with complex mesh designs, varying thickness and materials without manufacturing restraints. The performance of 3D printed spacers have been previously evaluated in reverse osmosis (RO) and ultrafiltration (UF) processes [15-19]. These studies reported considerable enhancement in mass

transfer with 3D spacers compared to conventional feed spacers. Nevertheless, an invariable trade-off with spacers is pressure drop [18], which increases the energy consumption of the process. Even so, the significant enhancement in water recovery may potentially offset the overall energy consumption.

The application of 3D printed spacers for MD has not been explored in detail thus far. Most studies used computational fluid dynamics (CFD) simulations to evaluate the effect of spacer geometrical parameters such as orientation, filament diameter, and thickness to identify optimal spacers for MD [10, 13, 14]. For instance, Chang et al. [10] used CFD simulations to study transmembrane DCMD transfer mechanism using empty and spacer-filled channels. The simulations established the benefits of using spacers in DCMD for enhanced mass flux as well as heat transfer and these enhancement factors depended on both the spacer design as well as the operating parameters such as the Reynolds number. Taamneh and Bataineh [20] used CFD simulations to evaluate the performance of DCMD with thick spacers with varied filament orientation (angle) and reported a positive increase of shear stress and the Nusselt number with spacer filaments oriented at 45° angles to the flow channel. Similarly, based on simulation results, Seo et al. [12] recommended zigzag spacers with symmetric circular designs and relatively high filament numbers as ideal to enhance permeate flux. These simulation studies imply the suitability of 3D spacers for MD application. In another study, Hagedorn et al. [21] highlighted that spacer characteristics such as porosity and spacer and filament thickness attributed to higher hydraulic diameter, which contributed towards turbulence (larger Reynolds) in DCMD. This factor is especially relevant for 3D printed spacers, as they can be fabricated at varied filament and spacer thickness. Thomas et al. [7] analyzed the performance of MD with 3D printed spacers and reported on enhanced permeate flux and overall heat transfer coefficient by up to 60% compared to commercial spacers. The performance enhancement was attributed to the significantly higher

turbulence induced by the maze-like interpenetrating design characteristics of triply periodic minimal surfaces (TPMS) used as the spacer topologies.

1.2 Potential of 3D printed spacers for fouling mitigation in MD

Apart from flux enhancement, spacer design can influence fouling and channel pressure drop in membrane processes. The presence of spacers enhances flow turbulence, which improves the mixing of the solution close to the membrane surface with the bulk solution. This, in turn, is expected to prevent foulant layer build-up on the membrane surface [22, 23]. A number of RO studies have established that spacer characteristics such as larger mesh size with varying/irregular filament thickness play a significant role in maintaining reasonable pressure drop, while creating high shear stress at the membrane surface, which is essential to avoid polarization and fouling issues [17, 24, 25]. These studies demonstrated the potential for fouling reduction using spacers with specific characteristics. 3D spacers can potentially meet such characteristics, given that the technology has the flexibility to fabricate spacers with complex features.

Organic fouling development in MD was systematically evaluated by a number of studies [26-28]. The severity of fouling in MD process appears to be significantly lower compared to pressure based membrane processes such as RO [2]. Nevertheless, the long-term operation can still lead to the accumulation of deposits on the membrane surface and pores, causing a decline of membrane permeability and it is a challenge to reverse fouled MD membrane even with chemical cleaning [1]. Further, the gradual membrane surface hydrophobicity reduction due to organic foulants deposition increases its susceptibility to wetting [1, 27]. This is especially relevant when MD is used to treat wastewater that contains a significant amount of organics [4, 29]. For instance, Wu et al. [29] reported significant membrane wetting when DCMD was used for fermented wastewater with high organic concentrations. Naidu et al. [4] demonstrated the potential of DCMD for wastewater RO concentrate treatment. Nevertheless, they also showed that the deposition of low molecular weight organics onto the membrane, due to the breakdown of humics at elevated

temperature, resulted in a considerable reduction in the membrane hydrophobicity [4]. The presence of spacers may potentially reduce fouling deposition onto the MD membrane. While Thomas et al. [7] indicated that 3D spacers show significant promise for treating brine solutions with high scaling tendency, a detailed evaluation of the implication of 3D spacers on fouling development in MD is still lacking. This study intends to bridge this gap.

Hence, this study aims to evaluate the role of 3D printed spacers (for simplicity referred to as 3D spacers hereafter) in improving the overall performance and fouling development in DCMD used for the treatment of wastewater RO concentrate. The influence of 3D spacer-filled channels for enhancing DCMD permeate flux, energy efficiency, as well as the implication on pressure drop, were evaluated. Specifically, in-depth analysis of organic fouling tendency in the presence of 3D spacers in DCMD used to treat wastewater up to high recovery rates (80-85% water recovery) was carried out. Factors such as accumulation of foulants onto the spacers and fouling reversibility with cleaning were also evaluated in detail.

2. Methodology

2.1 Materials

2.1.1 Membrane, chemicals, and feed solutions

A commercial polytetrafluoroethylene (PTFE) hydrophobic flatsheet membrane (General Electric, US) with nominal pore size, porosity, and membrane thickness of 0.22 µm, 70–80% and 179 µm, respectively [4] and total effective area of 40 cm^2 was used for all DCMD experiments.

DI water was used as a feed solution in the baseline tests. Baseline tests were conducted to evaluate the performance of DCMD with empty and spacer-filled channels at varied feed temperatures and flow velocities. The influence of spacers on organic fouling development in DCMD was tested using model humic solution as well as actual wastewater RO concentrate. The latter was obtained from a water reclamation plant of Sydney Olympic Park Authorities. Key

characteristics of this wastewater RO concentrate are summarized in **Table 1**. Model humic solution at a concentration of 20.3±0.7 mg/L was used to represent only the organic contents of the actual wastewater RO concentrate (**Table 1**) without any inorganic salts. Actual wastewater RO concentrate was used in this study to represent wastewater with both organic contents as well as inorganic salts.

Humic acid (Sigma-Aldrich, USA) and citric acid (Sigma-Aldrich, reagent grade) were used to prepare the simulant feed solution and chemical cleaning solution, respectively. The model humic acid solution was prepared by mixing 500 mg/L humic acid powder in deionized (DI) water with continuous stirring for 24 h. The pH of the final solution was not adjusted to ensure that the natural organic characteristics are unaltered. The humic acid stock solution was filtered (0.45 μm Millipore filter) to remove suspended solids and thereafter stored at 4 °C.

Furthermore, to critically determine the impact of organic contents in a mixed constituent, a condition of reduced organics with actual wastewater RO concentrate was used in this study. To achieve this condition, granular activated carbon (GAC) (from James Cumming & Sons Pty Ltd, MDW4050CB, particle size range 430 - 600 μm) was mixed (120 rpm) at 5.0±0.2 g/L with wastewater RO concentrate (24 h) to adsorb the organic contents, following the approach of our previous work [4] . Upon batch adsorption, the wastewater RO concentrate was filtered (0.45 μm millipore filter) to exclude suspended solids. The batch absorption using GAC significantly reduced the organic contents in actual wastewater RO concentrate to less than 2 mg/L while maintaining the inorganic salt contents.

Table 1 Characteristics of wastewater RO concentrate obtained from Sydney Olympic Park water reclamation plant [4].

Parameter	Value
Total dissolved solids (TDS)	1500.3±1.4 mg/L
Turbidity	0.2±0.1 NTU

Parameter	Value
pH	8.0±0.3
Dissolved organic carbon	20.3±0.7 mg/L
Ca	97.0±2.3 mg/L
Mg	69.0±1.6 mg/L
Na	448.5±3.2 mg/L
K	66.9±4.1 mg/L
SO_4	184.4±5.7 mg/L
Cl	611.4±3.3 mg/L
Hardness as $CaCO_3$	429.7±6.1 mg/L

2.1.2 Spacers

In this study, one commercial spacer and two types of 3D spacers were used. The commercial spacer (FILMTEC™) was diamond shaped (45° filament angle) with a porosity and thickness of 0.85 and 0.79 mm respectively, and made of polypropylene. The 3D spacers were designed based on TPMS resulting in a sheet-based transverse Crossed Layer of Parallel (tCLP) spacer and a skeletal-based Gyroid spacer. More details about TPMS shapes and their governing mathematical equations can be found elsewhere [7, 18]. The designs were modeled using computer-aided design software and then 3D printed by selective laser sintering technique. The unit cell representation of the selected TPMS spacer designs is presented in Fig. 1. The 3D tCLP spacer design consists of protrusions that create microchannels aligned perpendicular to the feed flow direction. This design feature was considered to create maximum flow disruption and resultantly increased turbulence. The specifications of the 3D spacers and their images are presented in **Table 2** and **Fig. 2,** respectively. The adaptation of TPMS is especially beneficial in minimizing the contact area between the membrane and spacer, which is essential to avoid flow restrictions and flow dead zones formation [16].

Table 2 Characteristics of 3D printed spacers.

Structure	Surface Area	Volume	Voidage	Hydraulic

design	(mm^2)	(mm^3)	(%)	Diameter (mm)
tCLP	14786	1067	88	1.2
Gyroid	10709	1471	84	1.4

180

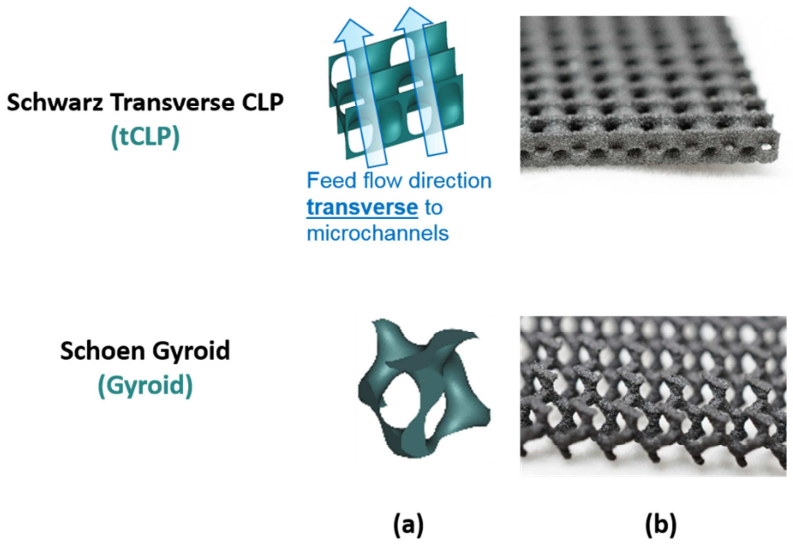

181

182 **Fig. 1** 3D printed TPMS spacer design features presented as **(a)** representative volume element,

183 and **(b)** photographic images (profile view)

184

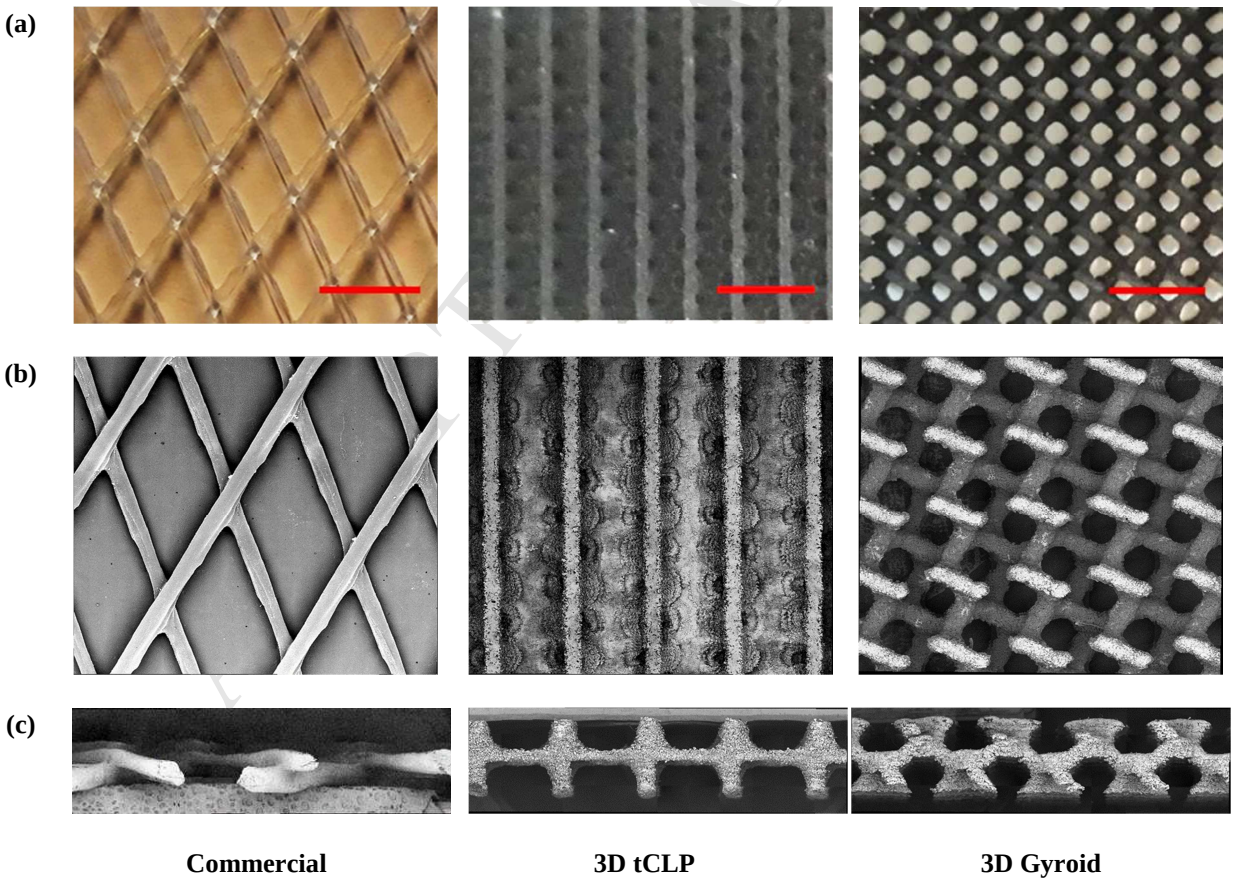

185 **Fig. 2** Commercial spacer and 3D printed spacers (tCLP and Gyroid) (a) photographic images

186 (image scale bar = 0.5 cm) **(b)** SEM image (top view) **(c)** SEM image (cross section).

2.2 Direct Contact Membrane Distillation (DCMD)

The spacer performance was evaluated in a closed looped bench scale DCMD system containing an acrylic membrane module (**Fig. 3**). The module length and width were 8.10 cm × 5.10 cm, respectively, with a channel depth of 0.23 cm.

Gear pumps (Cole-Parmer, model 75211-15, United States) were used to direct both the permeate (deionized (DI) water) and feed solution into the membrane channel in countercurrent flow at velocity (v_f and v_p) ranges of 0.1-0.3 m/s. Pressure variation at the feed inlet and outlet were recorded using pressure gauges placed at the feed inlet and outlet channel. A jacketed feed vessel coupled with a heating system was used to vary the feed solution temperature (T_f) from 45.0±2.0 ºC to 65.0±2.0 ºC while the permeate solution temperature (T_p) was maintained at 22.0±2.0 ºC for all experiments. Temperature at the inlet and outlet of the feed and permeate flow channels close to the membrane module was recorded using temperature sensors. The average feed and permeate membrane surface temperature profiles were obtained through these values. Heat losses on the feed side were determined based on the feed inlet to outlet temperature difference and as a function of the feed flow rate and constants (specific heat capacity = 4.2 kJ/kg.K; water density =1000 kg/m^3).

The permeate flux obtained across the active membrane area and latent heat of vaporization (2345.5 KJ/kg) were used to determine the latent heat transferred. The system energy efficiency was calculated based on the latent heat transferred over the heat losses at the feed side (detailed in **Section S1**).

DCMD experiments were carried out until 85% water recovery, equivalent to a reduction of the initial feed volume from 1.7 L to approximately 0.25 L or up to the point of significant permeate flux decline. An electronic balance was used for recording the weight changes in the permeate tank throughout the operation duration. The permeate flux computed as the ratio of permeate volume (L) increment over operation duration (h) and unit membrane area (m^2) was reported as L

212 m^{-2} h^{-1} (LMH). The permeate flux was represented as a function of the water recovery rate as well
213 as volume concentration factor (VCF). The VCF (defined as the ratio of initial to final feed
214 solution volume) indicates the extent of feed solution volume reduction achieved by DCMD.
215 DCMD with empty and spacer-filled channels were carried out with a number of feed solutions
216 from DI water for baseline evaluations followed by model humic solution as well as wastewater
217 RO concentrate for detailed analysis on the influence of spacers on fouling phenomena. The same
218 spacer design was used in both the feed and permeate channels for each DCMD experiment with
219 the spacer-filled channels.
220

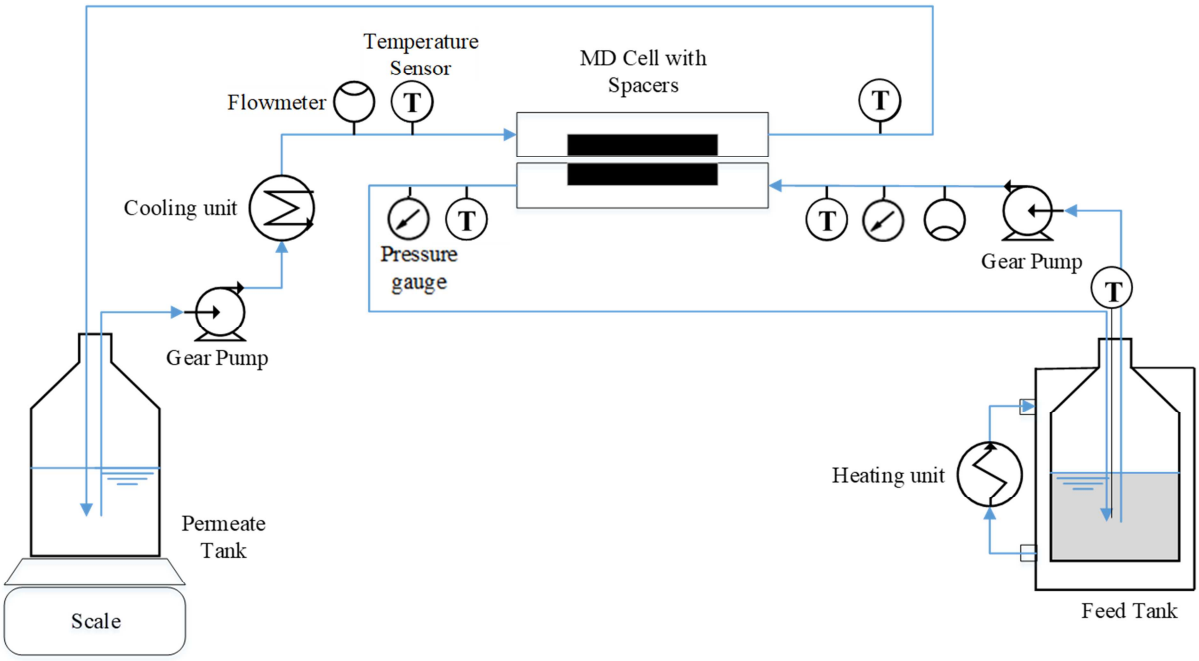

221
222 **Fig. 3** DCMD experimental setup.
223
224 The overall salt removal efficiency of DCMD was determined by measuring the conductivity and
225 pH value of the feed and permeate solution before and after DCMD operation, using a portable
226 multimeter (HQ40d, HACH, US). Inductively coupled plasma-mass spectrometry (ICP-MS,
227 Agilent 7900, US) was used to measure the concentration of each individual cation in the
228 wastewater RO concentrate. For organic removal efficiency, the initial and final permeate and feed

229 solutions (humic acid concentrations and wastewater RO concentrate) upon DCMD operation
230 were analyzed by a total organic carbon (TOC) analyzer (Analytik Jena multi N/C® 3100).
231
232 **2.3 Fouling reversibility with membrane cleaning**
233 **2.3.1 Batch membrane cleaning**
234 The effectiveness of cleaning the membrane as an approach to reverse membrane fouling was
235 evaluated using DI water as well as a chemical solution (0.1% citric acid). For this reason, small
236 portions of the used membranes were places in falcon tubes with 20 ml of cleaning solution. The
237 falcon tubes were stirred in a flat shaker at 120 rpm for 24 hours. Upon air drying, the membrane
238 contact angle was analyzed.
239
240 **2.3.2 Cleaning-in-place**
241 Cleaning-in-place (cleaning the membrane and spacer while in the module) was carried out to
242 emulate membrane maintenance and fouling mitigation in an actual operational scenario, upon
243 wastewater RO concentrate treatment. Cleaning-in-place was carried out with water cleaning
244 (flushing 300 mL of DI water through membrane module using the same operating flow velocity,
245 0.13 m/s) as well and chemical cleaning (0.1% citric acid with water flushing). Acid cleaning was
246 carried out by recirculating acid (20 mins at a low flow velocity of 0.08 m/s to achieve sufficient
247 contact time with the membrane) followed by water flushing (to neutralize the acid residues) (200
248 ml at 0.13 m/s). Cleaning-in-place is pertinent to establish the reuse capacity of both the
249 membrane as well as the 3D spacer.
250
251 **2.4 Characterization techniques**

252 **2.4.1 Organic Characterization**

253 Organic characterization of the feed and permeate solution, as well as membrane foulant, was
254 established using liquid chromatography with organic carbon detection (LC-OCD) [4, 30]. To
255 evaluate the organic characteristics deposited on the used MD membrane, foulant residues were
256 extracted from the membrane into MQ water based on the procedure of our previous studies [4,
257 27].

258

259 **2.4.2 Membrane characterization**

260 Changes in membrane characteristics before and after the DCMD experiments were evaluated in
261 terms of surface hydrophobicity and morphology. Membrane surface hydrophobicity was
262 measured using contact angle. Contact angle measurement was carried out at the end of each
263 experiment (upon drying the used membrane) together with a virgin membrane as a control
264 measure for the instrument setting. The contact angle measurements were conducted using a water
265 droplet goniometer (Theta Lite). Further, the surface morphology and element contents of the
266 membranes (virgin and used upon DCMD experiments) were examined using scanning electron
267 microscope (SEM) integrated with energy-dispersive spectroscopy (EDS) as described in a
268 previous study [4].

269

270 **3. Results and discussion**

271 **3.1. Baseline study**

272 The DCMD performance with and without spacer-filled channels was evaluated. For the baseline
273 study, DI water was used as the feed and permeate solution. The average DCMD permeate fluxes
274 obtained with varying operating conditions are presented in **Table S1**.

275

276 **3.1.1 Permeate flux performance**

277 In an empty channel (i.e., no spacer condition), increasing the bulk feed temperature from 45 to 65
278 °C (at a fixed flow velocity of 0.08 m/s) enhanced the permeate flux by 200% from 7.68±0.92
279 LMH to 24.26±1.45 LMH (**Fig. 4a**). In this study, temperature losses at the membrane feed side
280 were evaluated by measuring the temperature difference at the channel inlet and outlet (**Section 2**).
281 With the increase of bulk feed temperature, a higher feed temperature loss was observed due to the
282 large quantity of heat required for vaporizing liquid at the feed side of the membrane surface [9].
283 As a result of the temperature loss, only minimal energy efficiency increment was achieved with
284 the increase of permeate flux (**Fig. 4a**).
285 Meanwhile, at similar operating condition (feed temperature of 55 °C and flow velocity of 0.08
286 m/s), the permeate flux increased significantly by 63% (20.78±1.24 LMH) with commercial
287 spacer-filled channel, and by more than 200% (30.62±1.36 LMH to 36.06±1.09 LMH) with 3D
288 printed spacers as compared to that with empty channel (12.67±1.87 LMH) (**Fig. 4b**). More
289 importantly, the scenario of increasing the feed temperature to achieve higher permeate flux
290 invariably resulted in higher feed temperature losses, which compromised the energy efficiency.
291 The approach of spacer-filled channels was especially favorable in achieving both higher permeate
292 fluxes and energy efficiency.
293 Upon comparing the performance of DCMD with different spacers, the 3D spacer-filled channels
294 achieved 30-70% higher permeate fluxes compared to commercial spacer-filled channels under
295 similar operating conditions (**Fig. 5a**). This could be attributed to the smaller hydraulic diameter
296 of the 3D spacers (**Table 2**) and the channels/protrusions aligned perpendicular to the feed flow
297 such as in 3D tCLP spacer. A smaller hydraulic diameter increases the flow velocity and Reynolds
298 number. This, in turn, increases turbulence, resulting in higher mass transfer. Amongst the 3D
299 spacers, tCLP achieved 15-24% higher permeate fluxes compared to that with the Gyroid spacer.
300

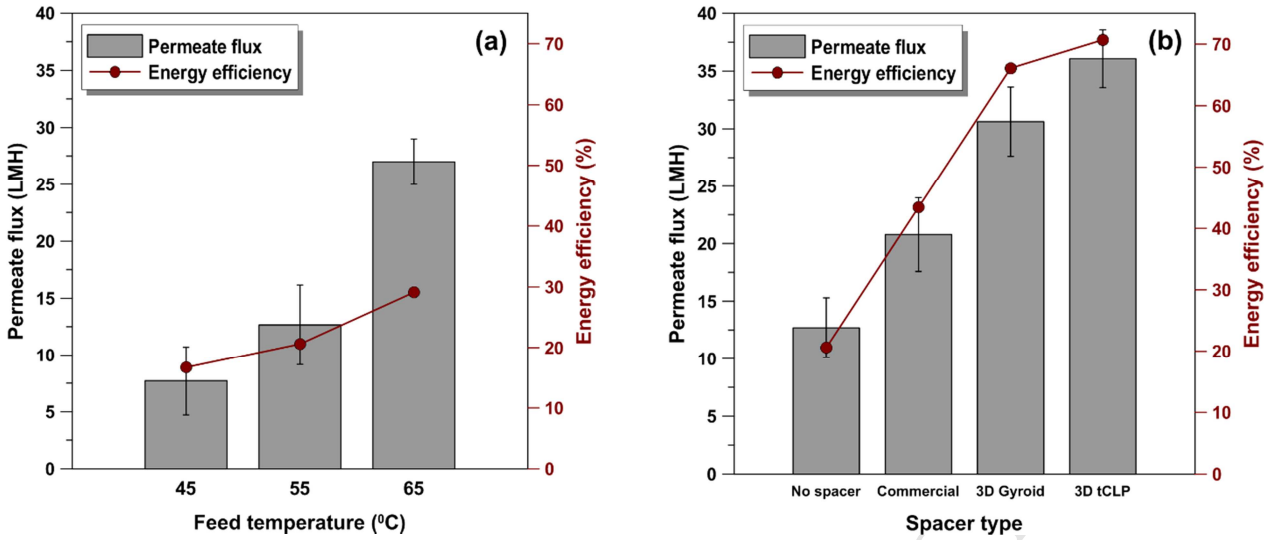

Fig. 4 Baseline performance of DCMD with **(a)** empty channel at T_f of 45.0±2.0 to 65.0±2.0 °C **(b)** empty and spacer-filled channels at T_f of 55.0±2.0 °C (v_f, v_p = 0.08 m/s; T_p = 22.0±1.5 °C).

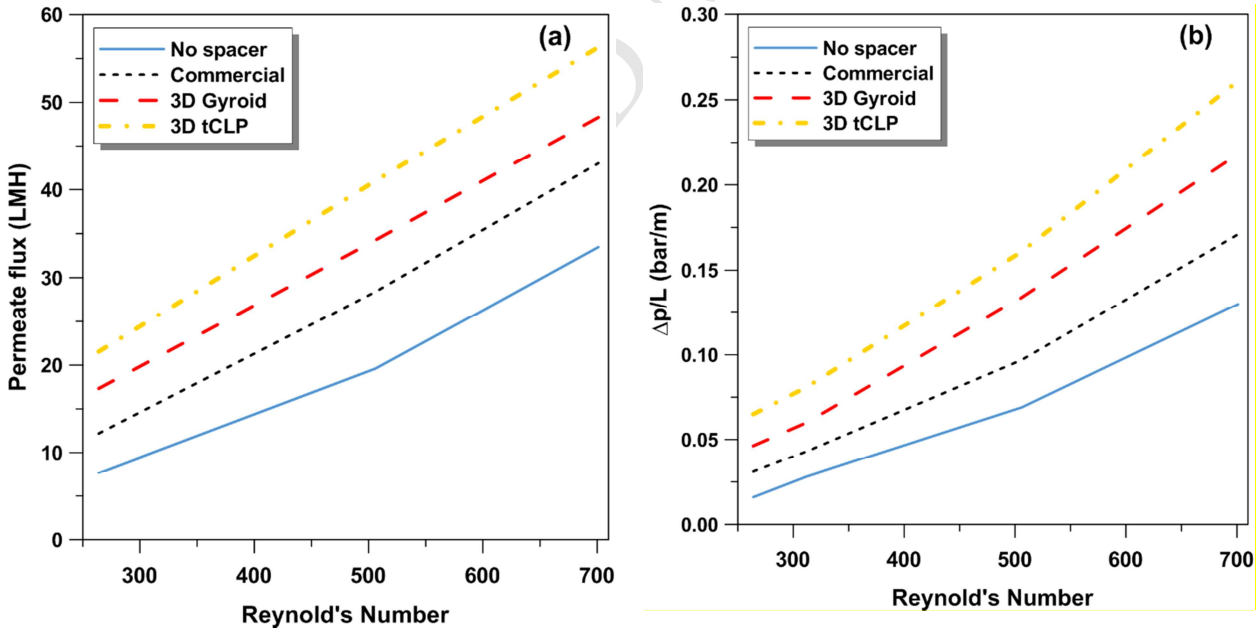

Fig. 5 Performance of empty and spacer-filled channel at varying flow velocities based on **(a)** permeate flux **(b)** channel pressure drop (figure trend line derived from experimental data from **Table S1**).

3.1.2 Channel pressure drop

Pressure drop is an inevitable trade-off associated with spacer application. The results of this study showed a trend of channel pressure drop increment in the ranges of 0.02–0.07 bar/m up to 0.13-0.25 bar/m as the flow velocity was increased (represented by Reynolds number) for both empty and spacer filled channels (**Fig. 5b**). The same trend of increasing pressure drop with flow velocity and Reynolds number was reported in previous MD studies [20, 21]. For instance, a previous MD study [21] showed that pressure drop in spacers could range from as low as 0.008 bar/m to over 1.0 bar/m depending on the flow velocity as well as spacer characteristics. A 48-200% increment in channel pressure drop was observed with spacer-filled channels compared to an empty channel. Higher drag force in the presence of spacers is associated with the higher channel pressure drop [12, 20, 21]. This apart, spacer characteristics such as spacer hydraulic diameter also influences the degree of channel pressure drop. Hagedorn et al. [21] demonstrated the inverse correlation of channel pressure drop and spacer hydraulic diameter, in which, reduced flow velocity associated with higher hydraulic diameter of the spacer resulted in lower channel pressure drop. Likewise, in this study, the channel pressure drop with Gyroid spacer (hydraulic diameter of 1.6 mm) was lower compared to the tCLP spacer (hydraulic diameter of 1.4 mm). In addition to the hydraulic diameter, another spacer characteristic that influences the feed channel pressure drop is the flow attack angle [31]. The flow attack angle of the spacer is the angle formed between the spacer strands and the fluid flow direction. In the tCLP design, the microchannels of the spacer are aligned perpendicular to the flow direction creating maximum disruption to the approaching fluid. However, with increasing flow attack angle, the pressure drop also increases. This explains the higher permeate flux and pressure drop observed with the tCLP spacer. Thus, based on the combined effects of flux enhancement and channel pressure drop, the Gyroid spacer demonstrated an overall improved performance over the commercial spacer.

3.2 Influence of spacer design on organic fouling mitigation

The baseline results established that the incorporation of spacers in DCMD enabled an improvement in permeate flux by maintaining low temperature polarization. The results also highlighted that at increased flow velocity, a higher permeate flux was achieved. However, at increased flow velocity, a trade-off of channel pressure drop is inevitable, especially in the presence of spacers. Based on all these factors, a DCMD operational setting of 55 °C feed temperature and 0.13 m/s flow velocity was decided upon for the subsequent tests to evaluate the influence of spacers on organic fouling development.

3.2.1 Process performance

DCMD tests were conducted for empty and spacer-filled channels using organic (humic acid) feed solution. Permeate flux results were compared in terms of the normalized flux (J/J_o). The obtained initial permeate fluxes (J_o) of 20.2±2.3 LMH (empty channel), 27.1±1.7 LMH (commercial spacer-filled channel), 37.5±1.3 LMH (3D Gyroid spacer-filled channel) and 44.2±2.4 LMH (3D tCLP spacer-filled channel) were in line with the baseline permeate flux results discussed earlier. For both empty and spacer-filled channels, the flux performance was relatively consistent over the majority of the experiment duration followed by a marginal decline towards the end of the experiment **(Fig. 6)**. A similar pattern of marginal decline in permeate fluxes was reported in previous studies [26, 28]. In MD, organic foulant tends to predominantly deposit onto the membrane surface and minimally on the membrane pores, due to the vapor pressure driving force rather than applied pressure. As a result, only marginal flux decline was observed. **Fig. 6b** highlights the improved performance duration achieved with the incorporation of 3D spacers. Owing to the enhanced flux performance, both the 3D spacers were are able to achieve the targeted 85% water recovery within a shorter duration of MD operation i.e. 50 to 80% of the operational duration needed with that of the commercial spacer. Additionally, the final flux

decline with the 3D Gyroid spacer (12%) was slightly lower to that obtained with the commercial spacer (17%) and empty channel (16%).

These results suggest that 3D spacer-filled channels were able to improve MD process performance. Further, in order to ascertain the influence of spacers on organic deposition onto the MD membrane, evaluations were carried out to study the organic mass deposition, characteristic of the organic compounds (LC-OCD analysis) and the condition of the used membranes such as the hydrophobicity and foulant deposition pattern.

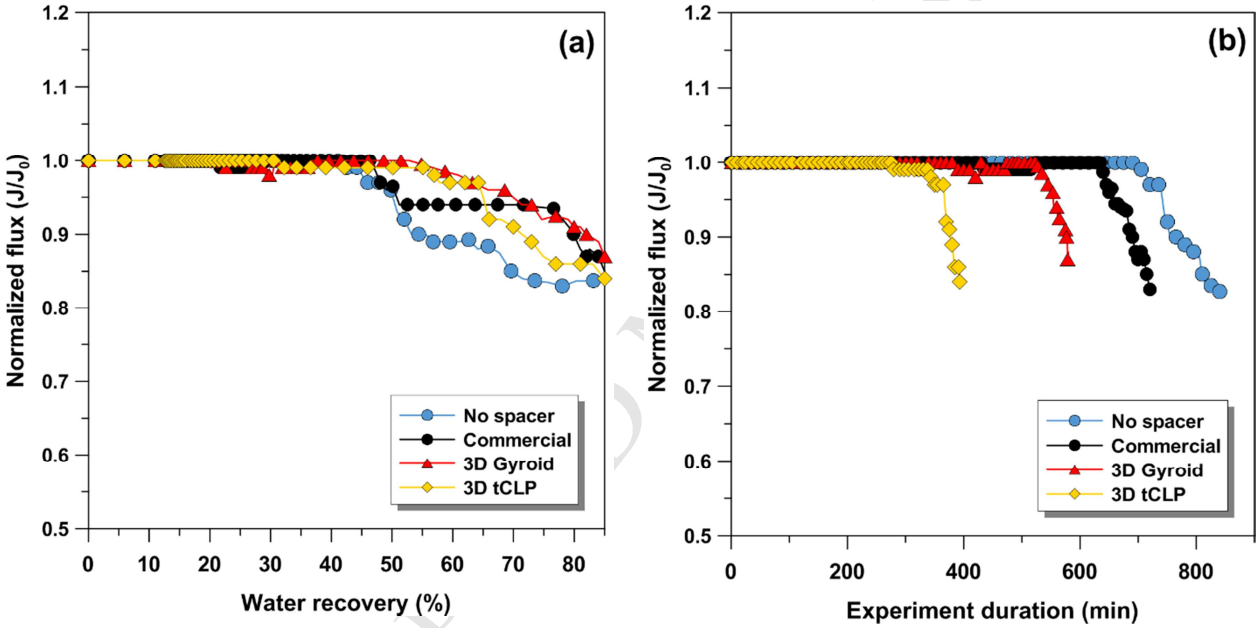

Fig. 6 Normalized DCMD permeate flux as a function of **(a)** water recovery and **(b)** experiment duration for both empty and spacer-filled channels. Conditions: Feed: model humic feed solution, T_f =55.0±2.0 °C, T_p= 22.0±2.0 °C, $v_{f,}$=v_p = 0.13 m/s).

3.2.2 Impact on foulant composition and adhesion

For all experimental conditions, a high-quality permeate was obtained throughout experiment duration. The conductivity (10-15 µS/cm) and organic contents (0.05- 0.10 mg/L) in the final permeate solutions were at trace levels and remained lower than that of the initial permeate

376 solutions, corresponding to 98-99% rejection of organics. The results indicated that the organics of
377 the feed solution did not penetrate into the membrane pores, as also supported by the marginal
378 permeate flux decline pattern (**Fig. 6**).

379

380 **Table 3** Feed solution organic mass balance for empty and spacer-filled channel DCMD operated
381 with model humic acid solution (initial feed solution volume -1.70 L; final feed solution volume -
382 0.25 L).

DCMD operating condition	Spacer type	Feed solution organic concentration (mg/L)		Feed solution organic mass (mg)		Organic mass reduction (%)
		Initial	Final	Initial	Final	
Empty channel	None	19.50±0.75	87.27±0.62	33.15±0.45	22.08±0.51	33.4
Spacer-filled channel	Commercial	19.50±0.75	102.96±0.71	33.15±0.45	26.05±0.60	21.4
	3D Gyroid	19.50±0.75	127.63±0.60	33.15±0.45	32.29±0.33	2.6
	3D tCLP	19.50±0.75	120.75±0.57	33.15±0.45	30.55±0.41	7.8

383

384 The dissolved organic content of the initial and final feed solution showed that the total organic
385 mass contents **(Table 3)** of the final feed solution with the empty channel and commercial spacer-
386 filled channels were 33% and 21% lower, respectively, than the expected value corresponding to a
387 seven-fold volume concentration (85% water recovery, VCF 6.7) of the organic contents in the
388 initial feed solution. On the contrary, the organic mass content of the final feed solutions with the
389 3D spacer-filled channels was closely similar to the expected value for seven-fold volume
390 concentration (85% water recovery, VCF 6.7) of the organic contents in the initial feed solution.
391 As only trace level of organics was detected in the permeate solutions, the reduced final feed
392 organic contents could presumably be attributed to organics deposition onto the feed channel and
393 adhesion onto the membrane as organic foulants. Considering that the same operating conditions
394 were applied for all the experiments, the organics deposition onto the feed channel would be
395 closely similar between empty and spacer-filled channels. However, based on the relatively lower
396 organic mass reduction of the feed solutions with 3D spacer-filled channels (3-8%), it would be

reasonable to infer that organic losses by deposition on the feed channel was minimal. Hence, the significant organic mass losses within the empty channel and commercial spacer-filled channels (21–33%) could most likely be attributed to organic foulant adhesion onto the membrane surface. Analysis of the organic characteristics of the initial feed solution affirmed that it predominantly consisted of humics (**Fig. 7**). Meanwhile, the final feed solutions of the empty and spacer-filled channels displayed some variation in organic characteristics. The final feed solution with empty channel showed a pattern of low humic peak with a substantially higher peak of building blocks. On the other hand, the organic characteristics of the final feed solution with spacer-filled channels maintained the same pattern as the initial feed solution, containing major peaks of humics with minor portions of low molecular weight (LMW) organics.

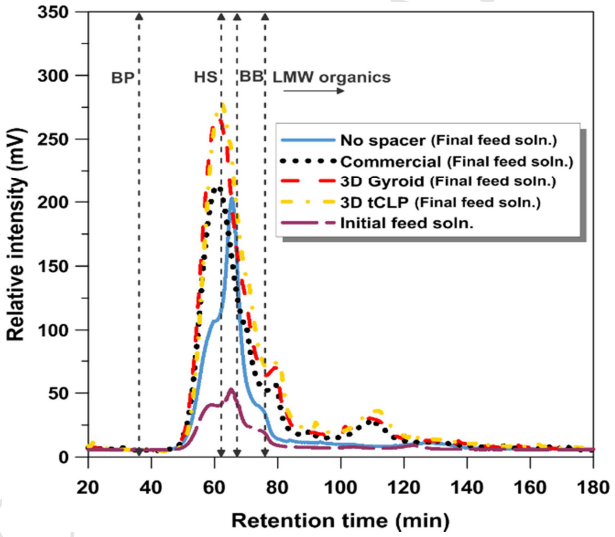

Fig. 7 LC-OCD chromatogram of initial and final humic feed solution for empty and spacer-filled channels (*BP- Biopolymers, HS- Humic substances, BB- Building blocks, LMW –Low molecular weight organics*).

Overall, the organic analyses of the feed solutions indicated that the presence of spacers in MD plays a significant role in organic fouling deposition pattern. Specifically, 3D spacers showed

414 significantly lower organic mass losses compared to commercial spacers. Overall, the organic
415 analyses of the feed solutions strongly indicated that the presence of spacers in MD play a
416 significant role in organic fouling deposition pattern. The 3D spacers, in particular, showed
417 significantly lower organic mass losses compared to commercial spacers. This observation was in
418 line with recent studies that analysed membrane fouling development with spacer filled channels
419 [32-34]. For instance, Wu et al. [34] explored the role of 3D spacers in membrane fouling
420 mitigating and highlighted that the design and orientation of 3D spacers resulted in lower fouling
421 by 25% compared to 2D spacers. Likewise, a simulation MD study observed that membrane
422 fouling occur on small isolated regions with spacer-filled channels compared to empty channel
423 attributed to uniform resident time and induction of the feed solution with the incorporation of
424 spacers [32]. Further, the feed solution organic characteristics results with LC-OCD imply that
425 spacers play a role in reducing the breakdown of humics to low molecular weight. To further
426 substantiate this observation and to understand the correlations between different spacer types and
427 organic fouling development in MD, organic characteristics of the foulant deposited onto the
428 membrane were analyzed.
429
430 Foulant deposition on the surface of the used membrane was visibly different with empty and
431 spacer-filled channels (**Fig. 8a**). The used membrane in the empty channel, showed significant
432 brown deposition while less deposition was observed in spacer-filled channels, especially with 3D
433 spacers. The SEM images (**Fig. 8b**) showed the presence of large colloid-like deposits on the used
434 membrane with the empty channel. Comparatively, only small and scattered deposits were
435 observed on the used membrane with spacer-filled channels.
436

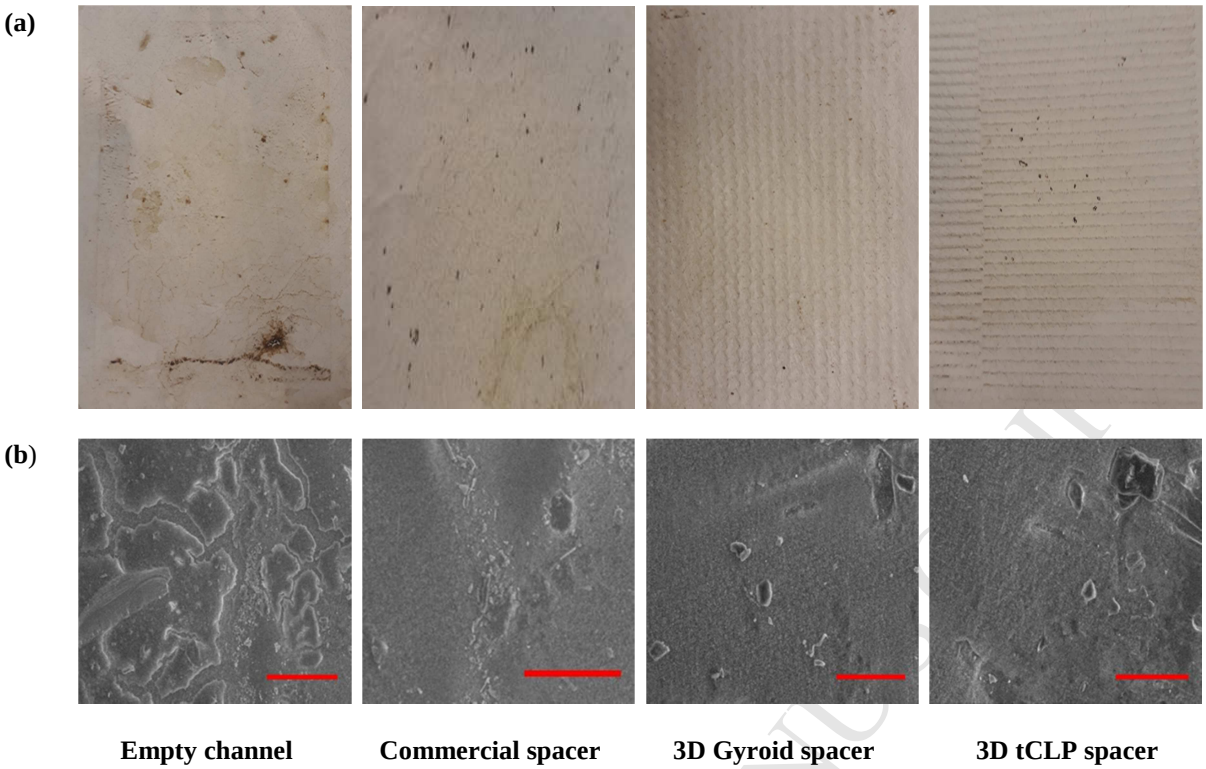

Fig. 8 Membrane surface morphology showing **(a)** foulant deposition on the used membranes **(b)** high magnified SEM images of the used membrane upon DCMD operation with empty and spacer-filled channels using model humic acid solution (SEM image scale bar = 100 μm).

The hydrophobicity of the virgin and used membrane surfaces were measured using water contact angle. The used membrane with empty channels showed the lowest water contact angle (70.2±1.3°), with a 50% hydrophobicity reduction compared to the virgin membrane (139.5±1.7°). Meanwhile, the used membranes with both commercial and 3D tCLP spacers showed similar hydrophobicity reduction in the range of 33-36%. On the other hand, the used membrane with 3D Gyroid spacer-filled channel retained the highest contact angle (only 13% hydrophobicity reduction) compared to the other used membranes, and its hydrophobicity was restored closely to the original condition with membrane cleaning (batch membrane cleaning). These results suggest that the low foulant deposition with 3D Gyroid spacer-filled channels enabled the membrane hydrophobicity to be restored closely to its original condition, even as the organic concentration in the feed solution was increased by more than 100 mg/L.

Table 4 Water contact angle of MD membrane (virgin, used and DI water cleaned) for empty and spacer-filled channel DCMD operation with model humic acid solution (Contact angle of new/virgin membrane =139.5±1.7°)

DCMD operating condition	Spacer type	Membrane water contact angle (°)	
		Used membrane (upon 85% water recovery)	*Cleaned membrane (DI water)
Empty channel	None	70.2±1.3	115.4±0.8
Spacer-filled channel	Commercial	87.5±1.5	129.7±1.7
	3D Gyroid	119.3±1.0	132.2±2.0
	3D tCLP	91.4±1.7	123.3±1.1

** Batch membrane cleaning (method as reported in Section 2.3.1)*

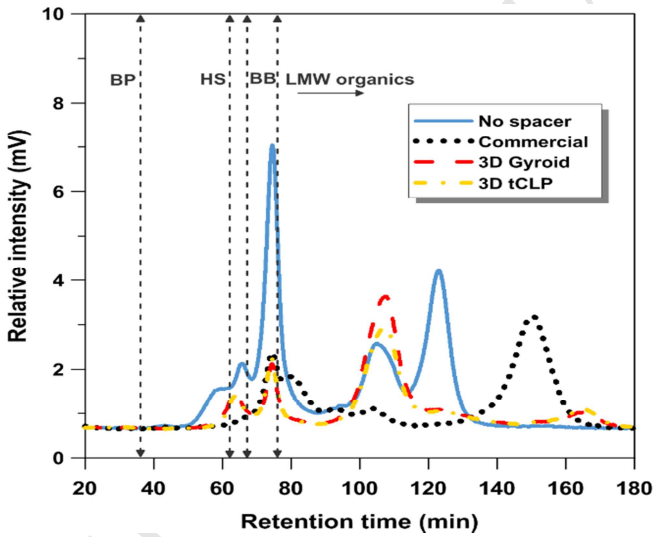

Fig. 9 LC-OCD chromatogram representing membrane foulant composition upon operation in empty and spacer-filled channels (*BP- Biopolymers, HS- Humic substances, BB- Building blocks, LMW –Low molecular weight organics*).

LC-OCD chromatograms of the membrane foulant (extracted from the membrane at the end of the experiment) are presented in **Fig. 9**. The results showed that the foulant deposited on the used membranes predominantly consisted of LMW organics. This was in line with the observation from

our previous studies that established the tendency of humics to break down to LMW organics in MD operation and thereafter, for LWM organics to deposit onto the hydrophobic membrane [4, 27]. This was attributed to the thermal condition in MD as well as the hydrophilic-hydrophobic attraction tendency between the foulant and the hydrophobic membrane. Given that the thermal condition was the same for all these four experiments, it is likely that the presence of the spacers may have acted as a barrier that reduced the hydrophilic-hydrophobic attraction between the MD membrane and the foulant. Therefore, the breakdown of humics was reduced in the scenarios with spacer-filled channels. Due to the barrier created by spacers, the tendency of humics breaking down to LMW organics in the feed solution was reduced, as observed with the feed solution organics characteristics analysis (**Fig. 7**). Hence, less LMW organics are deposited onto the membrane with spacer-filled channels. This tendency was especially apparent with 3D spacers and this could be due to their higher surface area coverage compared to commercial spacers (**Table 2**). The deposition of LMW organics onto the membrane is associated with membrane hydrophobicity reduction. In line with this, the substantially high LMW organics deposition on the used membrane with the empty channel resulted in significantly higher contact angle reduction (**Table 4**). The lower deposition of LMW organics on the membrane with spacer-filled channels could be due to the spacers acting as a barrier between the membrane and the concentrated feed solution.

3.2.3 Effect on fouling deposition patterns

Overall, the results indicated that the application of spacers (both commercial as well as 3D spacers) in MD resulted in lower fouling deposition compared to the empty channel. This could be related to the higher turbulence created by spacers. Higher turbulence disrupts the boundary layer close to the membrane (polarization effect) and enhances shear stress as established by a number of CFD modeling studies [12, 20, 32]. Higher shear stress is directly associated with reduced fouling deposition onto the membrane [18, 35].

Meanwhile, compared to the commercial spacer-filled channel, both the 3D spacers showed reduced fouling intensity, based on the lower foulant deposition on the membrane (**Table 3** and **Fig. 8**) as well as the lower reduction in membrane hydrophobicity (**Table 4**). This could be attributed to two factors, enhanced turbulence, and reduced dead zones. Firstly, compared to the commercial spacer, 3D spacers resulted in higher turbulence at the same feed velocity as reflected by the higher permeate fluxes achieved (**Fig. 5a**). The higher turbulence in 3D spacers is attributed to the non-uniform/varying filament thickness and smaller hydraulic diameter characteristics of the 3D spacers. In a simulation study, Taamenh and Bataineh [20] showed that significantly higher average shear stress was achieved by varying the top and bottom filament angle and when the angle of the spacers was closer to 90°. Hagedorn et al. [21] indicated that spacers with irregular filament surface and varying filament thickness contributed to better heat transfer efficiency and flow mixing. The higher turbulence and mixing with enhanced shear stress on the membrane surface with 3D spacers can be associated with the lower fouling deposition. Secondly, the factor of dead zone (restricted flow area) could likely contribute to higher fouling deposition onto the commercial spacer compared to the 3D spacers. Dead zone occurs when a spacer is in direct contact with the membrane which restricts flow velocity and accumulates deposits close to the membrane [14, 18]. Compared to a commercial spacer, 3D spacers are designed with TPMS topographies to generate surfaces (mean curvature of zero) with minimal contact area to the membrane [18]. The lower contact area to the membrane with 3D spacers reduces dead zone and results in lower fouling intensity compared to commercial spacers. Sreedhar et al. [18] observed higher biofouling development on RO membrane incorporated with commercial spacers than 3D spacers and this was attributed to the tendency of biofoulants to adhere especially around the contact area (dead zone) between the commercial spacer and the membrane.

In comparing the fouling performance with 3D spacer-filled channels, lower membrane fouling intensity was observed with Gyroid spacer over tCLP spacer on the basis of lower foulant mass

514 deposition on the membrane (**Table 3**) as well as restored membrane hydrophobicity (**Table 4**).
515 The variation in fouling deposition pattern between Gyroid and tCLP spacer could be explained in
516 terms of their different design characteristics. Lower surface area/volume (**Table 2**) value of
517 Gyroid (7.1 mm^{-1}) compared to tCLP (13.9 mm^{-1}) indicates that for a given channel volume the
518 Gyroid spacer offers a lower surface area for foulant adhesion and entrapment. This translates to
519 reduced dead zone and accumulation of foulants onto the membrane with Gyroid spacer. Spacer
520 voidage (porosity) is also an important characteristic that influences spacer performance.
521 However, in this case, the voidage for both the 3D spacers (Gyroid - 84%, tCLP - 88%) are closely
522 similar. On the other hand, in closely examining the design of both spacers, the skeletal-based
523 structure of the Gyroid spacer resembles a zigzag cubic shape with an infinite smooth surface.
524 This condition most likely creates a wave-like flow mechanism that does not potentially retain the
525 foulant. Comparatively, tCLP is a tetragonal sheet/layer which resembles a 'pocket' like shape. In
526 the case of tCLP, the channels or protrusions aligned perpendicular to the feed flow direction
527 creates high turbulence, which results in significantly higher permeate flux compared to Gyroid
528 (**Fig. 5a**). However, it is highly likely that the combination of this turbulence in the presence of the
529 pocket like shape promotes higher affinity for deposition of foulant onto the membrane as
530 depicted in **Fig. 10**. Likewise, a recent study evaluating the performance of vibrating 3D spacers,
531 reported on the superior membrane fouling mitigating by wave-like spacer compared to hill-like
532 spacer (a similar resemblance to the tCLP pocket like shape) [33]. In that study, Tan et al [33]
533 highlighted that although hill-like spacer does demonstrate higher local velocity, the protrusions of
534 wave like spacers creates large fluid movement, which enhances the overall shear along the
535 membrane, resulting in higher fouling mitigation.
536

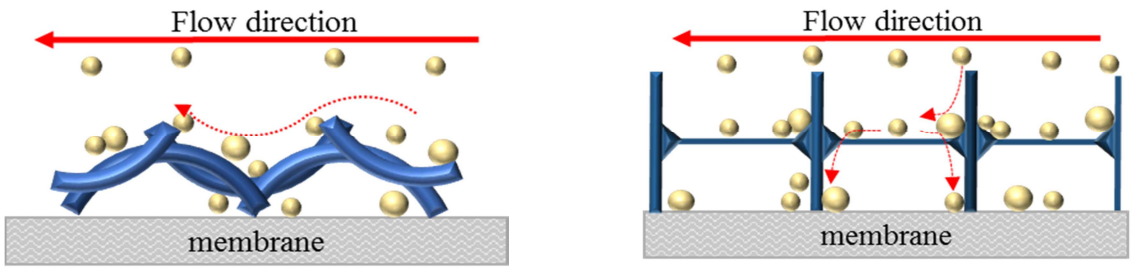

3D Gyroid spacer **3D tCLP spacer**

Fig. 10 Depiction of fouling deposition mechanism in DCMD with 3D spacer-filled channel.

In summary, although tCLP spacer-filled channel enables to achieve enhanced permeate fluxes compared to the other spacers, the organic fouling evaluation highlights that the superior fouling mitigation capacity is with 3D Gyroid spacer. Moreover, the lower channel pressure drop of 3D Gyroid spacer is an added advantage over the tCLP spacer.

3.3 Practical spacer application for wastewater treatment in MD

Based on the above factors, conditions that emulate actual treatment and fouling pattern (high organic contents in the presence of inorganic salts) is necessary to further substantiate and establish the role and practical application of 3D Gyroid spacer-filled channel towards fouling mitigation in MD. For this reason, evaluations were carried out with wastewater RO concentrate that contains high organics (similar to the model organic solutions) in a mixed composition with carbonate based inorganic salts (majorly Na, Ca, Mg) as listed in **Table 1**. At the same time, low organics wastewater RO concentrate (organic contents reduced through GAC adsorption) while maintaining the same inorganic salt concentration was used to compare and establish the role of organics in wastewater treatment with MD operation. Aspects such as permeate flux and quality and fouling pattern, potential pre-treatment requirement for enhancing the membrane durability as well as the adhesion of foulant onto the spacer and its reversible and reuse capacity was studied in detail.

557

558 **3.3.1 Process performance**

559 DCMD experiments with actual wastewater RO concentrate using both empty and Gyroid spacer-
560 filled channels achieved initial permeate fluxes of 19.5±1.7 LMH (empty channel) and 37.0±0.4
561 LMH (3D Gyroid spacer-filled channel for high and low organics), closely similar to the initial
562 fluxes with model organic solution (as reported in **Section 3.2.1).** However, at 85% water
563 recovery, permeate fluxes declined by 21-27% (**Fig. 11**), which was almost 2 times higher
564 compared to the 12-15% permeate flux decline rates with model organic solution (**Fig. 5**). Further,
565 the low organic wastewater RO concentrate (with 1.5±0.5 mg/L organics) exhibited similar
566 permeate flux trend as the actual wastewater RO concentrate (with 20.3±0.7 mg/L organics) (**Fig.**
567 **11**). These results suggest that, under the selected operating conditions, the inorganic ions at high
568 saturation (concentration) levels in wastewater RO concentrate played a more dominant role in
569 influencing the mass transport mechanism in DCMD rather than the organic contents.
570 In terms of permeate quality, the final permeate conductivity (18-22 uS/cm) increased slightly
571 compared to the initial permeate conductivity (10-15 μS/cm) for the case scenario of empty
572 channel. The rise in permeate conductivity reflected that partial wetting may have occurred. On
573 the other hand, the operation with Gyroid spacer-filled channels did not show any increment in
574 permeate conductivity, indicating the stability of the performance up to 85% water recovery rate.
575

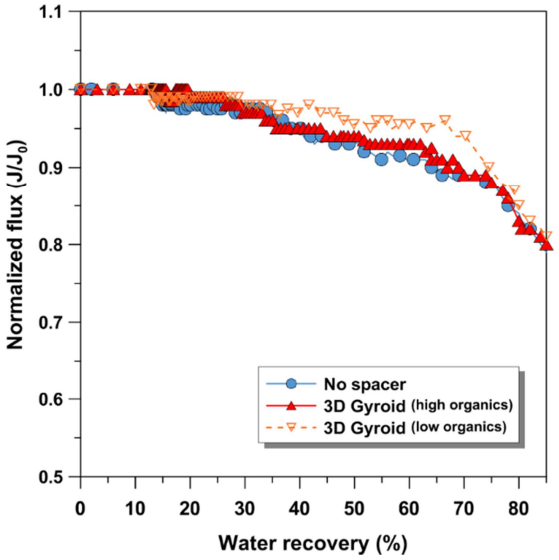

Fig. 11 DCMD permeate fluxes as a function of water recovery rate with empty and 3D Gyroid spacer-filled channels for wastewater RO concentrate treatment (T_f =55.0±2.0 °C, T_p= 22.0±2.0°C, v_f,v_p = 0.13 m/s) (Initial permeate fluxes: 19.5±1.7 LMH (empty channel) and 37.0±0.4 LMH (3D Gyroid spacer-filled channel for high and low organics).

The used membrane with the empty channel showed large mud colloid-like mixture of humics with inorganic salt crystals (**Fig. 12a**). The crystal shape and EDX element analysis established $CaCO_3$ as the main inorganic scalant. Comparatively, the used membrane with 3D Gyroid spacer displayed only small isolated regions containing colloidal foulant (**Fig. 12b**). In the case of low organic wastewater RO concentrate, the used membrane with 3D Gyroid spacer showed a different pattern with small scattered foulants that were loosely deposited onto the membrane (**Fig. 12c**).

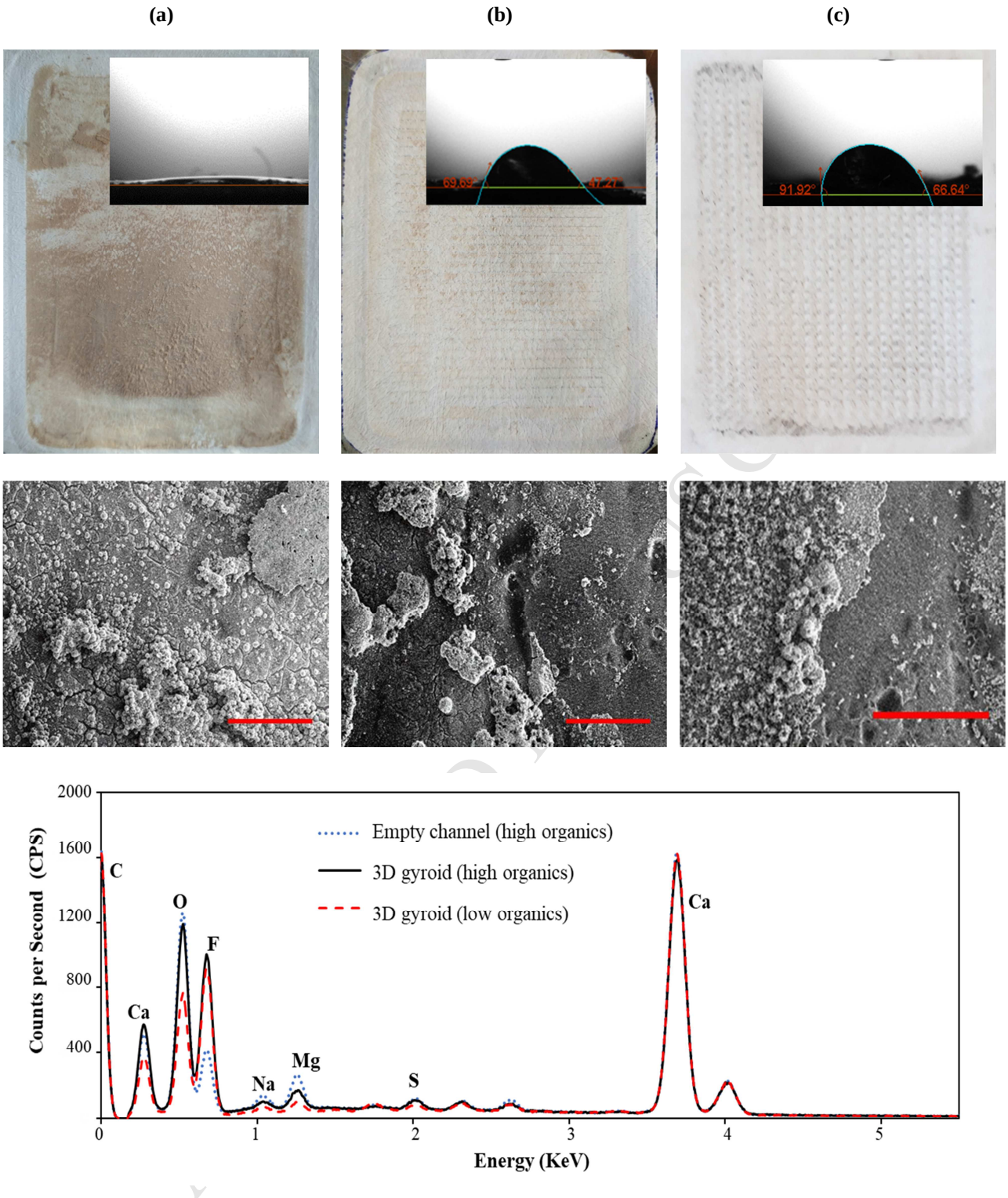

592 **Fig. 12** SEM-EDX and contact angle of the used membrane upon DCMD operation using
593 wastewater RO concentrate with **(a)** empty channel (high organics) **(b)** 3D Gyroid spacer-filled
594 channel (high organics) and **(c)** 3D Gyroid spacer-filled channel (low organics) (SEM image scale
595 bar = 300 μm).

Table 5 Water contact angle of the membranes (virgin, used and cleaned) for empty and 3D Gyroid spacer-filled channels DCMD operation with wastewater RO concentrate (Contact angle of new/virgin membrane =139.5±1.7°)

DCMD operating condition	Wastewater RO concentrate	Membrane water contact angle (°)		
		Used membrane	*Cleaned Membrane	
			DI water	Acid (0.1%)
Empty channel	High organics	5.2±2.7	7.4±0.8	10.4±0.8
3D Gyroid spacer	High organics	50.5±1.3	61.2±1.2	88.4±1.4
	Low organics	66.3±1.1	87.2±1.3	129.7±1.7

** Batch membrane cleaning (method as reported in Section 2.3.1)*

In terms of membrane hydrophobicity, the used membrane with empty channel resulted in more than 95-97% contact angle reduction compared to the virgin membrane (**Fig. 12a** and **Table 5**). The high hydrophobicity loss could be correlated to the partial wetting phenomena, based on the permeate conductivity increment as reported in **Section 3.3.1**. Moreover, membrane cleaning (batch membrane cleaning) with neither water nor acid could restore the membrane, indicating irreversible fouling. It is also worth mentioning that the high humic content as a single solute (**Table 4**) minimally affected the membrane hydrophobicity and the membrane condition was easily reversed with only water cleaning. These results suggest that treating and concentrating actual wastewater RO concentrate containing high humics mixed with inorganic ions is a challenge and would detrimentally affect the long-term performance of MD. Comparatively, the incorporation of 3D Gyroid spacer showed less hydrophobicity loss (57-60% contact angle reduction to the virgin membrane) (**Fig. 12b** and **Table 5**). This highlights the importance of 3D Gyroid spacer as a barrier that improved MD performance for wastewater treatment. Nevertheless, in attaining 85% water recovery (highly concentrated wastewater), reversing the foulant deposition and membrane hydrophobicity was still a challenge. Meanwhile, the combination of low organic wastewater RO concentrate with the incorporation of 3D Gyroid spacer was effective

in enabling to achieve high water recovery while restoring the membrane hydrophobicity with acid membrane cleaning. These results clearly indicated the necessity for a simple organic pre-treatment such as GAC filtration [4, 36] to maintain a stable MD performance in treating wastewater containing high organics.

Overall, the aforementioned evaluation highlighted the capacity of MD to treat wastewater RO concentrate and achieve high water recovery (85%) through a combination of GAC pre-treatment of wastewater (low organics wastewater) and the use of 3D Gyroid spacer-filled channels. Nevertheless, to establish the performance of MD for wastewater treatment, practical aspects such as cleaning-in-place (cleaning the membrane and spacer while it is in the module) as well as evaluation of membrane and spacer reuse capacity must be carried out. These aspects are discussed in the subsequent section.

3.3.2 Membrane and spacer reuse capacity

Three repeated MD cycles with low organic wastewater RO concentrate using the same membrane and 3D Gyroid spacer were carried out to establish the performance of MD for wastewater treatment. At the end of each cycle, cleaning-in-place (cleaning the membrane and spacer while it is the module) with water and chemical (0.1% citric acid with water flushing) was carried out to determine the reuse capacity of both the membrane as well as the spacer.

The results showed the capability of MD incorporated with 3D spacers to achieve high water recovery (85%) while maintaining stable permeate fluxes with low organic wastewater RO concentrate in three repeated cycles with cleaning-in-place (**Fig. 13)**. However, compared to the water membrane cleaning (final average contact angle = 87.2±1.7°), acid membrane cleaning was effective in maintaining the membrane hydrophobicity (final average contact angle = 130.7±1.7°) close to the virgin membrane (average contact angle =139.5±1.7°) (**Fig 14**). Likewise, the SEM

images showed the presence of visible foulant deposition on the membrane with DI water cleaning.

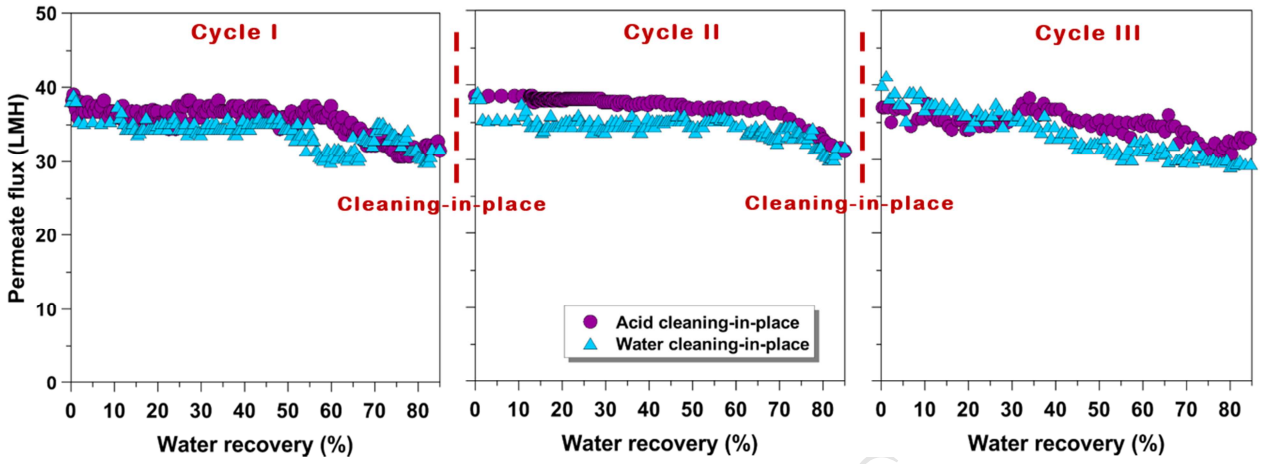

Fig. 13 Repeated cycles of DCMD with 3D Gyroid spacer-filled channel using low organics wastewater RO concentrate with cleaning-in-place (DI water and citric acid) at the end of each cycle.

Meanwhile, minimal deposition was visible on the acid cleaned membrane (closely resembling the virgin membrane). It is also worth mentioning that the membrane contact angle results with the cleaning-in-place were closely similar to the batch membrane cleaning (**Table 5**), indicating the suitability of a simple cleaning-in-place approach for maintaining the membrane in MD operation. Both the cleaning-in-place and batch membrane cleaning results indicated the necessity for a simple acid membrane cleaning for reversing foulant deposition and maintaining the membrane durability to achieve repeated cycles of MD operation for wastewater treatment.

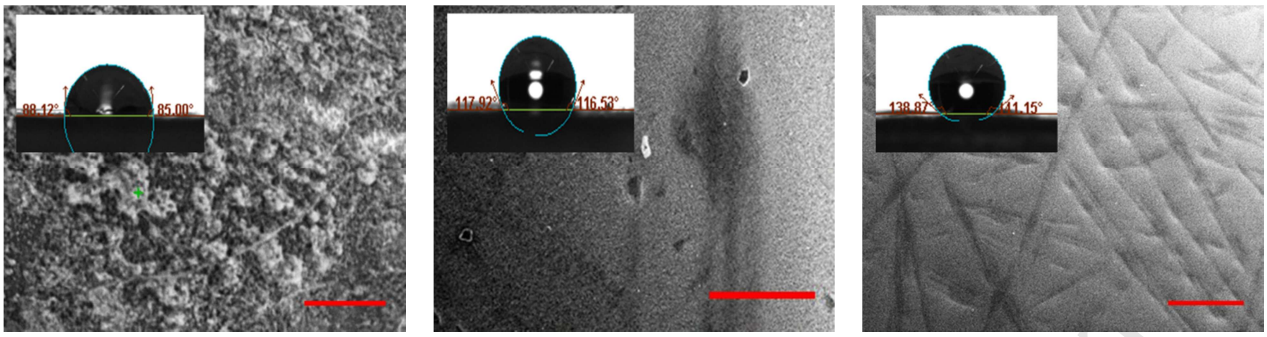

Water cleaning **Acid cleaning** **Virgin membrane**

655 **Fig. 14** Condition of the used membranes after three repeated DCMD cycles (low organic
656 wastewater RO concentrate treatment feed solution with 3D Gyroid spacer-filled channels) upon
657 cleaning-in-place with water and acid compared to the virgin membrane (SEM image scale bar =
658 200 μm).

659

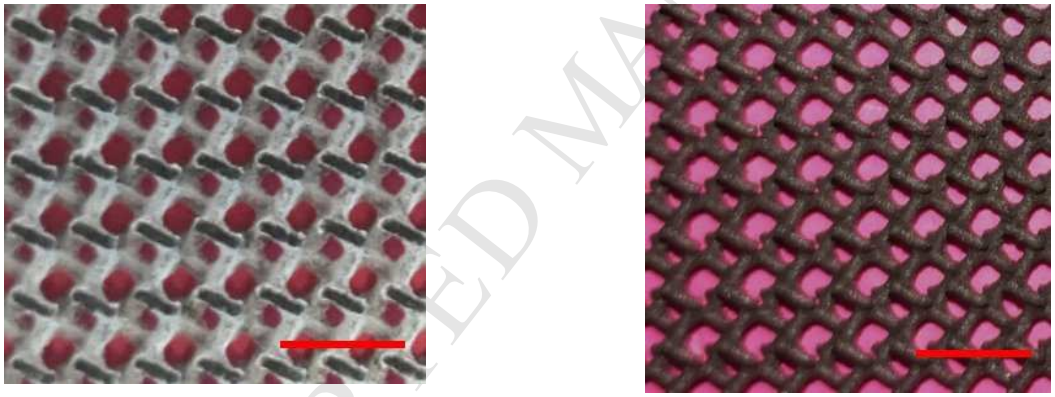

(a) **(b)**

660 **Fig. 15**. Condition of spacer (a) upon wastewater RO concentrate operation (b) upon cleaning in
661 place in DCMD (image scale bar = 0.5 cm)

662

663 Foulant deposition on the 3D Gyroid spacer was evident from its condition observed upon DCMD
664 operation (**Fig. 15a**). This is because the spacer acts as a barrier between the concentrated feed
665 solution and the membrane, which is favorable in reducing foulant deposition onto the membrane.
666 Nevertheless, inevitably, foulant tends to deposit onto the spacer. Hence, it is highly pertinent to
667 evaluate foulant reversibility and reuse capacity of the spacer. The results of the study showed

668 minimal foulant deposition (**Fig. 15b**) on the spacer used for three repeated cycles of MD
669 operation. This established the effectiveness of a simple cleaning-in-place for reversing foulants
670 on the spacer. The ease of reversing foulant on the spacer could be attributed to the spacer design
671 and material type that tend to repel foulant from adhering strongly on it. The reverse fouling and
672 reuse capacity of the 3D Gyroid spacer established its suitability to be incorporated in MD for
673 enhancing its performance for wastewater treatment.
674

675 **4. Conclusion**

676 This study evaluated the influence of 3D printed spacers in improving MD performance and
677 organic fouling development for treating wastewater. Overall, the results of the study highlighted
678 that:

679 • 3D spacers (Gyroid and tCLP) enabled to significantly enhance the performance of MD
680 (up to 200% increase in permeate flux and energy efficiency) compared to the empty
681 channel and up to 30-70% improved flux performance relative to the commercial spacer.
682 This was attributed to the unique features of 3D spacers that enhanced turbulence and mass
683 transfer; The trade-off of higher channel pressure drop with 3D spacers is inevitable.
684 • 3D Gyroid spacer showed better organic fouling mitigation capacity (based on the
685 membrane hydrophobicity and lower organic mass deposition) compared to tCLP and this
686 was attributed to the tortuous spacer design that can repel foulants;
687 • Treating and concentrating actual wastewater RO concentrate using MD without spacer
688 resulted in partial wetting with significant and irreversible foulant deposition onto the
689 membrane. This is attributed to the presence of organics in mixed constituents with
690 inorganic ions, as the membrane foulant with singe solute organics (humics feed solution)
691 was highly reversible;

692 - Repeated cycle of MD operation with a combination of low organics wastewater RO
693 concentrate with 3D Gyroid spacer and cleaning-in-place established the importance of (i)
694 a simple pretreatment to reduce organic content (ii) 3D spacers as a foulant barrier (ii)
695 cleaning-in-place, for achieving high recovery rate and stable long-term MD operation
696 with wastewater; and
697 - Cleaning-in-place established the foulant reversibility and reuse capacity of 3D Gyroid
698 spacer in MD.
699

700 ## Acknowledgments

701 The authors from University of Technology Sydney acknowledge the funding by Cooperative
702 Research Centre for Contamination Assessment and Remediation of the Environment (CRC
703 CARE) (Sustainable process for treatment of WWROC to achieve near zero liquid discharge).

704

References

[1] D.M. Warsinger, J. Swaminathan, E. Guillen-Burrieza, H.A. Arafat, J.H. Lienhard V, Scaling and fouling in membrane distillation for desalination applications: A review, Desalination, 356 (2015) 294-313.

[2] G.Naidu, S. Jeong, S. Vigneswaran, T.-M. Hwang, Y.-J. Choi, S.-H. Kim, A review on fouling of membrane distillation, Desalination and Water Treatment, 57 (2016) 10052-10076.

[3] A. Alkhudhiri, N. Darwish, N. Hilal, Membrane distillation: A comprehensive review, Desalination, 287 (2012) 2-18.

[4] G. Naidu, S. Jeong, Y. Choi, S. Vigneswaran, Membrane distillation for wastewater reverse osmosis concentrate treatment with water reuse potential, Journal of Membrane Science, 524 (2017) 565-575.

[5] G. Naidu, S. Jeong, M.A.H. Johir, A.G. Fane, J. Kandasamy, S. Vigneswaran, Rubidium extraction from seawater brine by an integrated membrane distillation-selective sorption system, Water Research, 123 (2017) 321-331.

[6] H.C. Duong, A.R. Chivas, B. Nelemans, M. Duke, S. Gray, T.Y. Cath, L.D. Nghiem, Treatment of RO brine from CSG produced water by spiral-wound air gap membrane distillation — A pilot study, Desalination, 366 (2015) 121-129.

[7] N. Thomas, N. Sreedhar, O. Al-Ketan, R. Rowshan, R.K. Abu Al-Rub, H. Arafat, 3D printed triply periodic minimal surfaces as spacers for enhanced heat and mass transfer in membrane distillation, Desalination, 443 (2018) 256-271.

[8] T.Y. Cath, V.D. Adams, A.E. Childress, Experimental study of desalination using direct contact membrane distillation: a new approach to flux enhancement, Journal of Membrane Science, 228 (2004) 5-16.

[9] G. Naidu, W.G. Shim, S. Jeong, Y. Choi, N. Ghaffour, S. Vigneswaran, Transport phenomena and fouling in vacuum enhanced direct contact membrane distillation: Experimental and modelling, Separation and Purification Technology, 172 (2017) 285-295.

[10] H. Chang, J.-A. Hsu, C.-L. Chang, C.-D. Ho, T.-W. Cheng, Simulation study of transfer characteristics for spacer-filled membrane distillation desalination modules, Applied Energy, 185 (2017) 2045-2057.

[11] J. Phattaranawik, R. Jiraratananon, A.G. Fane, Effects of net-type spacers on heat and mass transfer in direct contact membrane distillation and comparison with ultrafiltration studies, Journal of Membrane Science, 217 (2003) 193-206.

[12] J. Seo, Y.M. Kim, J.H. Kim, Spacer optimization strategy for direct contact membrane distillation: Shapes, configurations, diameters, and numbers of spacer filaments, Desalination, 417 (2017) 9-18.

[13] H. Yu, X. Yang, R. Wang, A.G. Fane, Analysis of heat and mass transfer by CFD for performance enhancement in direct contact membrane distillation, Journal of Membrane Science, 405-406 (2012) 38-47.

[14] M. Shakaib, S.M.F. Hasani, I. Ahmed, R.M. Yunus, A CFD study on the effect of spacer orientation on temperature polarization in membrane distillation modules, Desalination, 284 (2012) 332-340.

[15] C. Fritzmann, M. Wiese, T. Melin, M. Wessling, Helically microstructured spacers improve mass transfer and fractionation selectivity in ultrafiltration, Journal of Membrane Science, 463 (2014) 41-48.

[16] J.-Y. Lee, W.S. Tan, J. An, C.K. Chua, C.Y. Tang, A.G. Fane, T.H. Chong, The potential to enhance membrane module design with 3D printing technology, Journal of Membrane Science, 499 (2016) 480-490.

[17] A. Siddiqui, S. Lehmann, S.S. Bucs, M. Fresquet, L. Fel, E.I.E.C. Prest, J. Ogier, C. Schellenberg, M.C.M. van Loosdrecht, J.C. Kruithof, J.S. Vrouwenvelder, Predicting the impact of feed spacer modification on biofouling by hydraulic characterization and biofouling studies in membrane fouling simulators, Water Research, 110 (2017) 281-287.

[18] N. Sreedhar, N. Thomas, O. Al-Ketan, R. Rowshan, H. Hernandez, R.K. Abu Al-Rub, H.A. Arafat, 3D printed feed spacers based on triply periodic minimal surfaces for flux enhancement and biofouling mitigation in RO and UF, Desalination, 425 (2018) 12-21.

[19] W.S. Tan, S.R. Suwarno, J. An, C.K. Chua, A.G. Fane, T.H. Chong, Comparison of solid, liquid and powder forms of 3D printing techniques in membrane spacer fabrication, Journal of Membrane Science, 537 (2017) 283-296.

[20] Y. Taamneh, K. Bataineh, Improving the performance of direct contact membrane distillation utilizing spacer-filled channel, Desalination, 408 (2017) 25-35.

[21] A. Hagedorn, G. Fieg, D. Winter, J. Koschikowski, A. Grabowski, T. Mann, Membrane and spacer evaluation with respect to future module design in membrane distillation, Desalination, 413 (2017) 154-167.

[22] L. Fortunato, Y. Jang, J.-G. Lee, S. Jeong, S. Lee, T. Leiknes, N. Ghaffour, Fouling development in direct contact membrane distillation: Non-invasive monitoring and destructive analysis, Water Research, 132 (2018) 34-41.

[23] S. West, M. Wagner, C. Engelke, H. Horn, Optical coherence tomography for the in situ three-dimensional visualization and quantification of feed spacer channel fouling in reverse osmosis membrane modules, Journal of Membrane Science, 498 (2016) 345-352.

[24] Y. Gao, S. Haavisto, C.Y. Tang, J. Salmela, W. Li, Characterization of fluid dynamics in spacer-filled channels for membrane filtration using Doppler optical coherence tomography, Journal of Membrane Science, 448 (2013) 198-208.

[25] H.-G. Park, S.-G. Cho, K.-J. Kim, Y.-N. Kwon, Effect of feed spacer thickness on the fouling behavior in reverse osmosis process — A pilot scale study, Desalination, 379 (2016) 155-163.

[26] M. Khayet, A. Velázquez, J.I. Mengual, Direct contact membrane distillation of humic acid solutions, Journal of Membrane Science, 240 (2004) 123-128.

[27] G. Naidu, S. Jeong, S.-J. Kim, I.S. Kim, S. Vigneswaran, Organic fouling behavior in direct contact membrane distillation, Desalination, 347 (2014) 230-239.

[28] S. Srisurichan, R. Jiraratananon, A.G. Fane, Humic acid fouling in the membrane distillation process, Desalination, 174 (2005) 63-72.

[29] Y. Wu, Y. Kang, L. Zhang, D. Qu, X. Cheng, L. Feng, Performance and fouling mechanism of direct contact membrane distillation (DCMD) treating fermentation wastewater with high organic concentrations, Journal of Environmental Sciences, 65 (2018) 253-261.

[30] S.A. Huber, A. Balz, M. Abert, W. Pronk, Characterisation of aquatic humic and non-humic matter with size-exclusion chromatography – organic carbon detection – organic nitrogen detection (LC-OCD-OND), Water Research, 45 (2011) 879-885.

[31] A.R. Da Costa, A.G. Fane, D.E. Wiley, Spacer characterization and pressure drop modelling in spacer-filled channels for ultrafiltration, Journal of Membrane Science, 87 (1994) 79-98.

[32] J. Amigo, R. Urtubia, F. Suárez, Exploring the interactions between hydrodynamics and fouling in membrane distillation systems – A multiscale approach using CFD, Desalination, 444 (2018) 63-74.

[33] Y.Z. Tan, Z. Mao, Y. Zhang, W.S. Tan, T.H. Chong, B. Wu, J.W. Chew, Enhancing fouling mitigation of submerged flat-sheet membranes by vibrating 3D-spacers, Separation and Purification Technology, 215 (2019) 70-80.

[34] B. Wu, Y. Zhang, Z. Mao, W.S. Tan, Y.Z. Tan, J.W. Chew, T.H. Chong, A.G. Fane, Spacer vibration for fouling control of submerged flat sheet membranes, Separation and Purification Technology, 210 (2019) 719-728.

[35] H.S. Abid, D.J. Johnson, R. Hashaikeh, N. Hilal, A review of efforts to reduce membrane fouling by control of feed spacer characteristics, Desalination, 420 (2017) 384-402.

[36] S. Jeong, H. Bae, G. Naidu, D. Jeong, S. Lee, S. Vigneswaran, Bacterial community structure in a biofilter used as a pretreatment for seawater desalination, Ecological Engineering, 60 (2013) 370-381.

Supplementary Information

3D printed spacers for organic fouling mitigation in membrane distillation

Erik Hugo Cabrera Castillo, Navya Thomas, Oraib Al-Ketan, Reza Rowshan, Rashid K. Abu Al-Rub, Seongchul Ryu, Duc Long Nghiem, Saravanamuthu Vigneswaran, Hassan A. Arafat, Gayathri Naidu

S1 Energy Efficiency Calculation

The total heat exchanged by the feed (Q_f) within the MD module, represented by Eq. 1, is the input source of energy within the system which is calculated as the difference between the sensible heat of the incoming feed stream and the outgoing feed stream.

$$Q_f = \rho q C_w \left(T_{f,i} - T_{f,o}\right) \quad (1)$$

where ρ is the density of water, q is the volumetric feed flow rate, C_w is the specific heat capacity of water, $T_{f,i}$ is the temperature of the incoming feed water and $T_{f,o}$ is the temperature of the outgoing feed water.

The heat lost from the feed contributes to the heat transport through the membrane (inclusive of the latent heat accompanying the vapor flux (Q_v) and the heat conducted through the membrane) and the heat lost through the membrane module via conduction losses. As the membrane module is made from acrylic (low thermal conducitivity material), the conduction heat losses is assumed to be negligible. The latent heat accompanying the vapor flux through the membrane can be calculated as per Eq. 2:

$$Q_v = JA\rho H_v \quad (2)$$

where J is the water vapor flux through unit area of the membrane, A is the effective membrane area, and H_v is the latent heat of vaporization.

Thus, the system energy efficiency (η) was calculated as the ratio of the latent heat transferred through the memrbane and the heat losses at the feed side, indicated by Eq. 3.

$$\eta = \frac{Q_f}{Q_v} \quad (3)$$

858 **Table S1** Average DCMD permeate fluxes obtained with varying operating conditions

Flow Velocity (m/s)	Feed Temperature(°C)	Flux (LMH)			
		No spacer	Commercial	3D Gyroid	3D CLP
0.08	45	7.68±0.92	12.19±1.49	17.33±1.19	21.54±1.14
	55	12.67±1.87	20.78±1.24	30.62±1.36	36.06±1.09
	65	24.26±1.45	31.75±0.76	47.28±1.18	54.07±0.70
0.13	45	12.42±0.66	17.28±0.89	20.83±1.26	26.21±1.21
	55	19.60±0.88	28.40±1.69	37.26±0.91	43.99±0.70
	65	35.81±1.77	44.83±1.88	58.06±1.30	67.43±1.51
0.18	45	15.42±1.08	19.01±1.63	23.82±1.06	30.17±1.45
	55	28.48±1.79	32.90±1.53	42.28±1.44	49.29±1.12
	65	52.04±1.01	57.04±1.00	66.32±1.32	76.37±1.39

859
860
861
862
863
864
865
866
867
868
869
870
871
872
873
874
875
876
877

878

Highlights

- 3D spacers increased MD fluxes by 50-65% compared to a commercial spacer.
- Organics cause marginal flux decline but impact membrane hydrophobicity in MD.
- 3D Gyroid spacer with tortuous zigzag design was suitable for repelling foulants.
- MD with 3D Gyroid spacer achieved 85% water recovery from low organic wastewater.
- Cleaning-in-place and organic pre-treatment are vital for MD wastewater treatment.